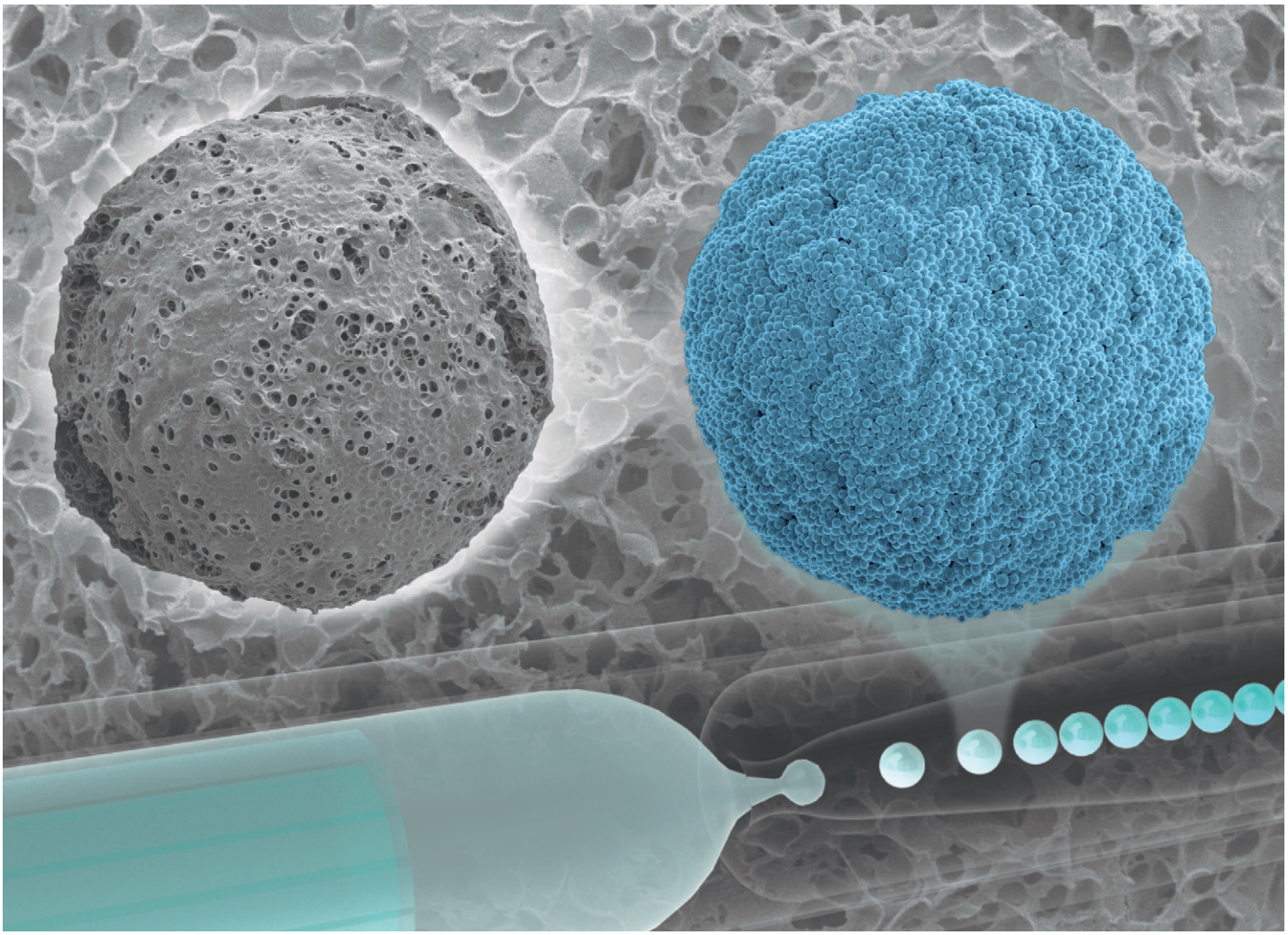

Featuring work from the Abolhasani Lab of the Department of Chemical and Biomolecular Engineering at North Carolina State University, which focuses on the development of enabling microfluidics and flow chemistry strategies toward addressing the environmental challenges of growing global energy demand.

Continuous Synthesis of Elastomeric Macroporous Microbeads

A solid templating porous particle synthesis strategy is coupled with microfluidic droplet generation for the synthesis of elastomeric macroporous microbeads. The developed microfluidic platform allows for the continuous on-chip synthesis of monodisperse silica-loaded polysiloxane microbeads followed by porogen removal via selective etching.

As featured in:

See Milad Abolhasani *et al.*, *React. Chem. Eng.*, 2019, **4**, 254.

ROYAL SOCIETY OF CHEMISTRY | Celebrating IYPT 2019

rsc.li/reaction-engineering

Registered charity number: 207890

Reaction Chemistry & Engineering

COMMUNICATION

View Article Online
View Journal | View Issue

Cite this: *React. Chem. Eng.*, 2019, **4**, 254

Received 30th August 2018,
Accepted 9th November 2018

DOI: 10.1039/c8re00189h

rsc.li/reaction-engineering

Continuous synthesis of elastomeric macroporous microbeads†

Jeffrey A. Bennett, Zachary S. Campbell and Milad Abolhasani *

Macroporous microbeads are synthesized by microfluidic production of silica-loaded polymeric microdroplets followed by porogen removal *via* selective etching. Microdroplets are produced in a flow-focusing microreactor to ensure monodispersity with uniform porogen loading. Effects of porogen size and polymer network density on the porosity and effective modulus of the microbeads are studied.

Macroporous microparticles have important applications in areas where enhanced surface area and rough surface topology are preferred over dense spherical microparticles.[1] The macroporous microparticles are utilized in applications ranging from catalysis[2] and selective adsorbents,[3] to enzyme immobilization,[4] drug delivery,[5] and cell growth scaffolding.[6,7] Porous monoliths have been considered as reactor packing[8] and catalyst scaffolds, but suffer from flow channelling, which is mitigated in particulate beds. Porous microparticles have been fabricated using a wide variety of materials (*e.g.*, ceramics, oxides, polymers, and hydrogels)[6,9–12] and methods (*e.g.*, emulsification,[13] templating,[14] and self-assembly) in both bulk[10] and flow reactors.[1,15,16] Crosslinked polysiloxane networks have been demonstrated to have tunable viscoelastic and surface properties[17,18] which can be varied to promote cell growth, as well as favourable biocompatibility and oxygen transport.[18] Porous particles of linear polysiloxanes have been synthesized using salt-induced osmosis of water microdroplets into the droplets of linear polysiloxane that are formed during the bulk emulsification process.[13] Despite the high degree of porosity, bulk emulsification methods have the downside of a very wide particle size distribution due to the uncontrolled breakup in the mechanical emulsification process. Over the past two decades, droplet-based microfluidic strategies – owing to precise control over the flow and reaction parameters – have been successfully utilized for continuous synthesis of a wide range of micro/nano structures.[19–24]

In this work, we demonstrate a microfluidic strategy for continuous synthesis of elastomeric macroporous microbeads with tuneable size and porosity. Depending on the intrinsic properties of the substrate material, different microfluidic approaches have been utilized to create macroporous beads. Such methods include fabrication of intrinsically porous beads through solvent removal and spontaneous phase separation,[25] as well as structural templating with immiscible fluids (basic and high-internal-phase emulsions (HIPE))[14,26] and solids (*e.g.*, salt, sugar, polystyrene, and silica).[3] Unique physicochemical properties of polysiloxanes limit the feasibility of the more conventional microfluidic approaches for forming macroporous beads. For example, (poly)hydromethylsiloxane (PHMS) is not compatible with spontaneous phase separation or solvent removal, as the network must be chemically crosslinked through hydrosilylation. Additionally, the lack of UV or thermal initiated crosslinking means that the PHMS microbeads must be formed with porogen present as the crosslinking reaction is occurring. During preliminary screening, it was found that the fluid-based templating of PHMS droplets had major drawbacks for continuous synthesis of macroporous microbeads, namely the stability and droplet size of the formed water-in-oil or gas-in-oil emulsions. The surfactant required to generate stable water-in-oil emulsions would cause immiscibility issues with the PHMS and crosslinker mixture, thus preventing the hydrosilylation catalyst from mixing with the polymer phase to begin crosslinking. Thus, solid porogens were considered as the templating material. The conventional sacrificial polystyrene (PS) microspheres were rejected due to their solubility in the PHMS crosslinking solvent (toluene), which would dissolve the PS microspheres before the PHMS could solidify into a porous network. Crystalline solids (*e.g.*, sodium chloride and sucrose) were rejected for similar reasons; the microscale particles would migrate to the fluid interface between the

Department of Chemical and Biomolecular Engineering, North Carolina State University, 911 Partners Way, Raleigh, USA.
E-mail: abolhasani@ncsu.edu; Web: https://www.abolhasanilab.com/

† Electronic supplementary information (ESI) available. See DOI: 10.1039/c8re00189h

nonpolar PHMS and the polar continuous phase (water) and promptly dissolve before the PHMS network could crosslink. However, mesoporous amorphous silica microspheres are insoluble in all the fluids used in the flow synthesis of elastomeric microbeads and can be removed selectively during post-processing. Potassium hydroxide (KOH) selectively etches the amorphous silica microspheres, leaving behind the porous PHMS scaffold. An overview of this process is shown in Fig. 1.

Experimental

In this work, building on our recently developed capillary-based microfluidic reactor for dense PHMS particles,[27] we developed a flow synthesis strategy (Fig. 2) for continuous production of porous silicone elastomer microbeads with tunable size and porosity.

Chemicals

(Poly)hydromethylsiloxane (PHMS) (average Mn 1700–3200), 1,5-hexadiene, platinum(0)-1,3-divinyl-1,1,3,3-tetramethly-disiloxane (Karstedt's Catalyst) (in Xylene, Pt-2 wt%), toluene (anhydrous, 99.8%), and sodium dodecyl sulfate (SDS), were purchased from Sigma Aldrich. A 500 molecular weight vinyl-terminated polydimethylsiloxane crosslinker (DMS-V03, hereafter V03) was purchased from Gelest Inc. Acetone and 2-propanol (IPA) were purchased from VWR Analytical. Silica gels (HPLC grade, spherical 5, 7.5, 10 and 20 μm APS, 120 angstroms) were purchased from Alfa Aesar. All chemicals were used as received. Deionized water was obtained in-house using a PURELAB Flex purification unit.

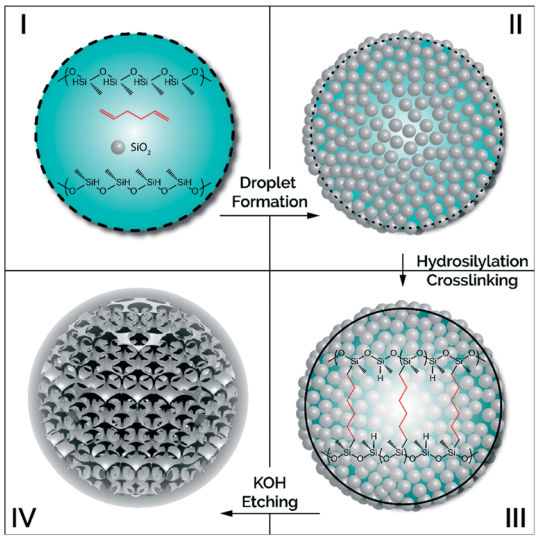

Fig. 1 (I) Major components of the microparticles: PHMS (polymer), 1,5-hexadiene (crosslinker), and mesoporous silica microparticles (porogen). (II) Liquid PHMS droplet loaded with silica microparticles produced by the flow-focusing microreactor. (III) Porogen-loaded PHMS microbead after crosslinking by hydrosilylation. (IV) Schematic of the formed macroporous microbead after selective removal of the solid porogen with chemical etching.

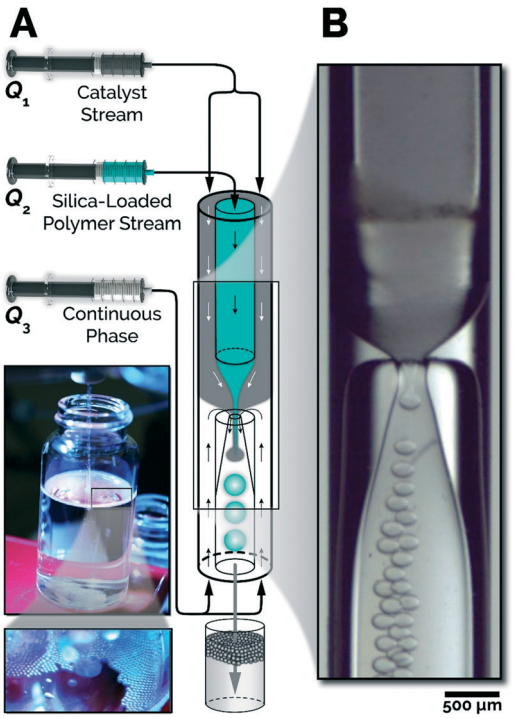

Fig. 2 (A) Schematic of the developed microfluidic platform for the continuous synthesis of the macroporous microbeads. The inset shows the microbead collection bath. (B) An image of the capillary-based flow-focusing microreactor utilized for the synthesis of elastomeric microbeads. Q_1 = 10 μL min^{-1}, Q_2 = 10 μL min^{-1}, Q_3 = 200 μL min^{-1}.

Experimental setup

The microfluidic platform, shown in Fig. 2, consists of a 3D coaxial flow-focusing microreactor (producing uniform microdroplets – the silicone networks), three syringe pumps (PHD ULTRA, Harvard Apparatus), and a collection bath.

The microreactor consists of two inner coaxial borosilicate glass capillaries (0.75 mm inner diameter, 1.0 mm outer diameter) with their tips separated by ~1 mm. Both inner capillaries are sheathed in an outer glass capillary (1.12 mm inner diameter, 1.5 mm outer diameter) resulting in two coaxial inner microchannels and two annular microchannels on either side of the gap. A full diagram of the necessary fluidic connections is shown in the ESI,† Fig. S1. The capillary-based microreactor constructed using off-the-shelf components offers advantages in cost and rapid prototyping compared to expensive custom microfabricated reactors. The inlet streams, including two dispersed and one continuous phase, are delivered into the microreactor using syringe pumps and gas-tight glass (dispersed phase) and stainless-steel (continuous phase) syringes. The inlet side inner microchannel contains a mixture of the polymer (PHMS), crosslinker (1,5-hexadiene or V03), solvent (toluene), and silica microspheres of selected sizes (from 1.6–10 μm), while the inlet side annulus contains a mixture of toluene and crosslinking catalyst to begin the hydrosilylation crosslinking on chip. Water and sodium dodecyl sulfate (SDS) are fed through the outlet-side

annulus as the continuous phase (with surfactant) for facile microdroplet breakup and stabilization until crosslinking is finished in the collection bath. The center microchannel of the outlet side is a flamed-tip constricted glass capillary (produced using a Narishige PC-10 capillary puller) to promote breakup of the polymer mixture jet into small droplets and carry them to the collection bath (filled with DI water) where the crosslinking is completed. Upon crosslinking of the in-flow generated droplets, spherical silicone elastomer microbeads filled with close-packed silica microspheres are formed. In the next step, the porogen (*i.e.*, mesoporous amorphous silica microspheres) is selectively removed using potassium hydroxide solution. When the silica loading inside the microbeads is close-packed, the etching process creates interconnected pores throughout the elastomeric microbead.

Reagent preparation

The precursor solutions were prepared as detailed in Table 1. The silica-loaded polymer precursor solution was prepared by mixing the polymer and crosslinker in the desired ratio (3 : 1 and 5 : 1 PHMS : crosslinker by mole basis). The viscosity of the polymer precursor solution was reduced by adding an organic solvent (toluene) prior to the addition of the silica microspheres. Silica microspheres of the desired size (1.6–10 μm) were then added to the polymer mixture until the mixture set into a colloidal gel (*i.e.*, vial could be inverted without flow). Next, an additional 25% v/v of the polymer was added to ensure the mixture could flow in the syringe, microreactor, and tubing and connections. The crosslinking catalyst concentration was precisely tuned to ensure prompt crosslinking of the microbeads in the collection bath to prevent possible coalescence during collection while ensuring the mixture remained a liquid during the in-flow mixing and breakup inside the flow-focusing microreactor. The crosslinking catalyst concentration (*i.e.*, crosslinking time) was tuned off-line using small (100 μL) batch gel tests. The maximum concentration of Pt in the polymer prior to the washing steps is ~40 μM which is significantly lower than EPA reported values of Pt toxicity (0.1 mmol kg^{-1})[28] or Pt catalyzed reactions.

DI water with 3 wt% SDS was used as the continuous phase to lower the surface energy of the polymer jet/water interface and promote breakup while preventing droplet coalescence before crosslinking in the collection vial.

Table 1 Different stream components of the flow-focusing microreactor shown in Fig. 2

Stream	Components	Purpose
Q_1	Toluene	Solvent and diluent
	Karstedt's catalyst	Crosslinking catalyst
Q_2	PHMS	Polymer
	1,5-Hexadiene or V03	Crosslinker
	Silica gel	Porogen
	Toluene	Solvent and diluent
Q_3	Water	Continuous phase
	SDS	Surfactant

Microdroplet formation

Before collection of the elastomeric microbeads, the flowrates of the various streams were adjusted to find a stable dripping flow regime, as droplet formation from a polymer-based liquid/solid colloid mixture is non-Newtonian. The main parameters adjusted were (a) the ratio between the two inlet streams (*i.e.*, $Q_1 : Q_2$) to vary the loading of silica within the microdroplet and the viscosity of the microdroplet mixture, and (b) the total dispersed phase and continuous phase flow rates (Q_1 + Q_2 & Q_3) which control the velocity of the two fluids at the flow-focusing orifice and the resulting flow regime within the microreactor.

Microparticle collection

The silica-loaded PHMS microdroplets were collected in a large water bath to prevent contact between droplets before crosslinking was finished. The microreactor outlet was inserted into the water in the collection vial to eliminate dripping of the microreactor effluent into the collection vial and its potential effects on the droplet shape and porogen loading. Following collection, the microdroplets were allowed to crosslink in the water bath for 24 h to ensure complete crosslinking before washing. Upon completion of the crosslinking step, the elastomeric microbeads were filtered (Whatman 1004-100 20 μm pores) and washed to remove the surfactant (SDS). The microbeads washing protocol involved two rinses with DI water followed by two rinses with isopropanol and two rinses with acetone. After washing, the microbeads were dried at room temperature.

Selective removal of solid porogen

Following washing and drying of the silica-loaded elastomeric microbeads, the silica microspheres were selectively removed from the elastomer network by etching with 1 M KOH. A small amount of acetone (~100 μL per mL) was added to the 1 M KOH solution to reduce the surface tension and achieve complete porogen removal. When pure KOH is used, surface tension can prevent penetration of the etchant into small pores within the silica-loaded and semi-etched elastomeric microbeads. The PHMS microbeads were left in the etchant solution for 2 h to achieve complete removal of the solid porogen. Following the solid porogen removal, the washing and drying protocol was repeated, and the samples were prepared for further analysis using electron microscopy and X-ray microcomputed tomography.

Porosity characterization

SEM imaging. Following the synthesis, drying, and porogen removal steps, the elastomeric microbeads were characterized using scanning electron microscopy (FEI Verios 460 L Field Emission SEM and Hitachi 3200 N Variable Pressure SEM) to evaluate the degree of silica loading, particle size, and size dispersity as well as the pore network inside the porous microbeads.

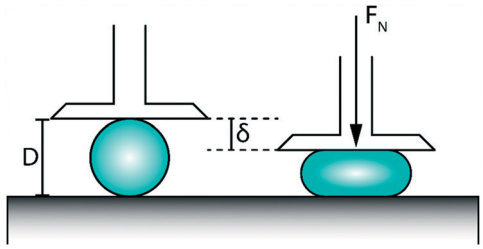

Fig. 3 Schematic of the modulus test setup using a parallel plate configuration. Normal force and plate separation distance were measured over a compression and relaxation of an individual microbead.

MicroCT imaging. Samples of the synthesized elastomeric microbeads (both etched and unetched) were subjected to a micro-computed tomography (μCT) scan (Nikon XTH 225 ST) with a voxel size of ~6 μm to verify that the mesoporous silica microspheres were completely etched without causing structural damage to the elastomeric microbeads in the etch bath.

Mechanical tests: effective modulus

Effective moduli of the different PHMS microbeads (control, silica-loaded, and porous beads) were determined using a rheometer (TA Instruments DHR3) in parallel plate configuration to measure force *vs.* axial compression of individual microbeads. The data was then fit to Hertz's equation,[14,29]

$$F = \frac{E \times D^{\frac{1}{2}}}{3\left(1-\nu^2\right)}\left(D-H\right)^{\frac{3}{2}} \quad (1)$$

and normalized by the microbead diameter,[14] resulting in the following equation

$$\frac{F}{D^2} = \frac{E^*}{3}\left(\frac{\delta}{D}\right)^{\frac{3}{2}} \quad (2)$$

where F is the measured axial force, D is the uncompressed microbead diameter, δ is the compression distance, E is the bulk modulus, ν is Poisson's ratio, and E^* is the effective modulus defined as $E/(1-\nu^2)$. The schematic of the moduli measurement setup is shown in Fig. 3.

Results

In the first step, we studied the degree of porogen packing and efficacy of the selective porogen removal using SEM imaging. Fig. 4 shows monolayer, single particle, cross section, and surface morphology of the synthesized elastomeric

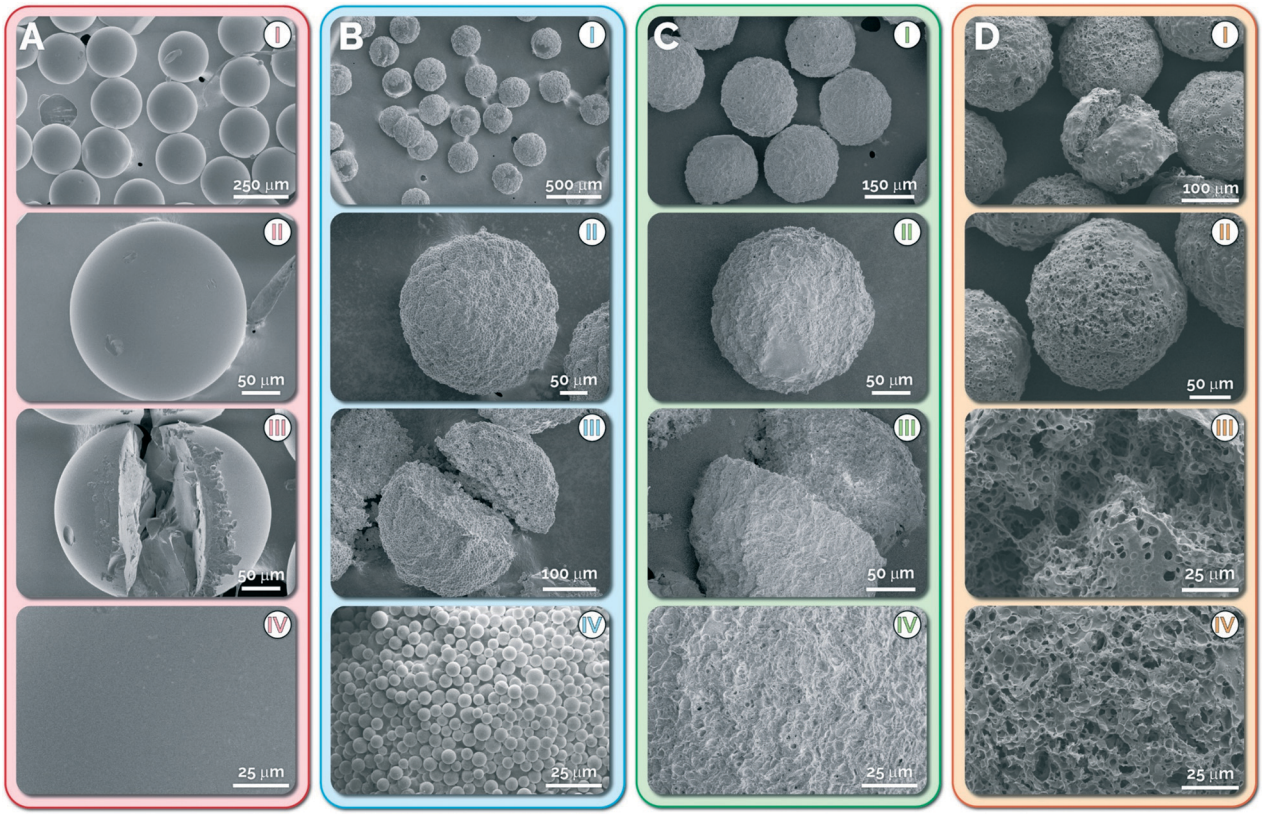

Fig. 4 SEM images of PHMS microbeads (A) without silica gels ($Q_1/Q_2/Q_3$ = 5/10/200 μL min^{-1}), (B) with 5 μm silica gels ($Q_1/Q_2/Q_3$ = 10/10/300 μL min^{-1}), (C) after selective etching of the silica particles ($Q_1/Q_2/Q_3$ = 10/10/300 μL min^{-1}), (D) and etched particles using a divinyl-terminated PDMS crosslinker ($Q_1/Q_2/Q_3$ = 8/12/50 μL min^{-1}). (I) Monolayer microbeads; (II) single intact microbead; (III) inside the elastomeric microbeads; (IV) surface morphology of the microbeads.

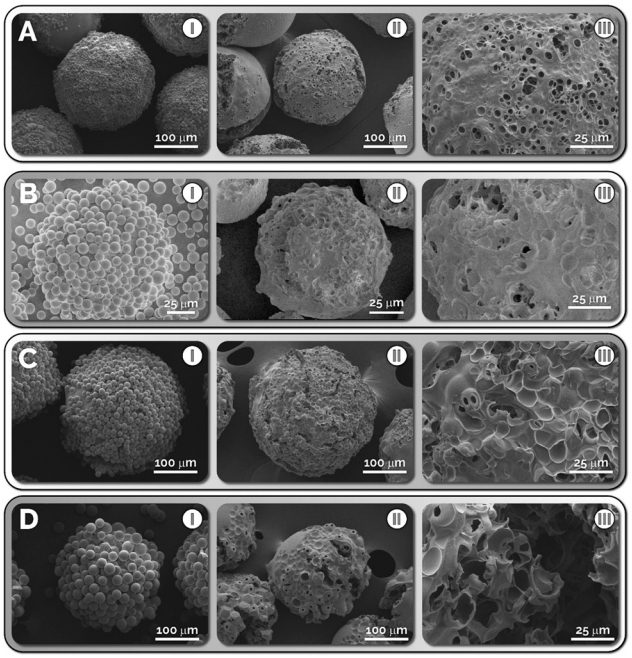

Fig. 5 PHMS microbeads synthesized with (A) 5, (B) 7.5, (C) 10, and (D) 20 μm sized mesoporous silica microspheres using 5 : 1 PHMS : V03. SEM images of (I) silica-loaded microbeads, (II) single macroporous microbead, and (III) surface morphology of the macroporous PHMS microbeads. Flowrates Q_1, Q_2, and Q_3 in μL min^{-1}: (A) 4/12/250, (B) 8/14/150, (C) 5/10/100, and (D) 8/18/200.

microbeads. The mesoporous silica microspheres used in the microreactor are on the order of 50–100× smaller than the flamed-tip opening to mitigate any possible clogging of the outlet capillary. It was observed that flow rate ratios of silica-loaded polymer stream to catalyst stream greater than 1 : 1, resulted in stable polymer jet formation and breakup with uniform porogen loading inside each droplet (see ESI† Video M1). Using SEM imaging, it was determined that the produced monodispersed PHMS microbeads were uniformly loaded with close-packed silica microspheres, which were completely removed upon etching with KOH (Fig. 4 Biii and Ciii). In the next step, we investigated the effect of varying the crosslinker length on the degree of porosity within the macroporous microbeads. As shown in Fig. 4C and D, switching from the hexadiene crosslinker to the divinyl PDMS crosslinker enhanced the pore interconnectivity and surface porosity of the resulting particles. Compared to the hexadiene crosslinker, the vinyl-terminated PDMS makes the polymer network stronger and less brittle due to the additional length and flexibility offered by the PDMS chains. The molar density of V03 is much lower than the hexadiene crosslinker due to the high molecular weight (500 *vs.* 82 g mol^{-1}) and bulky PDMS chain. The stronger network allows improved survival of the thin-walled pores during the filtering and SEM plating process. The PHMS microscaffolds produced by our microfluidic method showed an excellent monodispersity (CV < 5%, see Fig. S2 and S3 in the ESI†) compared to the polysiloxane microbeads synthesized using bulk emulsification techniques (20% < CV < 100%). The CV of the produced microbeads begins to dramatically increase (~12% with 20 μm silica) with the size of silica particles as they begin having a significant influence on the dynamics of droplet formation at the flamed-tip opening. Silica-loaded droplets break off from the bulk fluid by necking down, which is more dramatically affected when larger silica particles are present in the necking region.

Next, we studied the effect of porogen size on the degree of porosity of the resulting elastomeric macroporous microbeads. Varying the size of the mesoporous silica microspheres loaded into the droplets allows for size tuning of the resulting macropores within each PHMS microbead (Fig. 5). As the size of the silica microspheres increases, the size of the resulting macropores increases as well, leading to large voids and interconnected spaces. However, increased porogen size negatively affects the stability of droplet breakup in the microreactor and can lead to rapid separation of the colloidal silica suspension in the precursor syringe, resulting in heterogeneous flow of silica microspheres. Small perturbations in the jet breakup dynamics introduced by varying porogen size can have a significant impact on the range of flow rates that result in monodisperse dripping. Minimizing the porogen size introduces smaller breakup disturbances, but the desired pore size for a given application must be considered.

In order to study the penetration depth of the etchant solution into the porogen-loaded elastomeric microbeads, high-resolution μCT imaging was performed on dried porogen-loaded (control) and macroporous microbeads. High-resolution μCT imaging provides information about the internal structure of PHMS microbeads without the need for destructive analysis by cutting into the microbeads. Fig. 6 and ESI† video M-2 show reconstructed μCT images of the tested

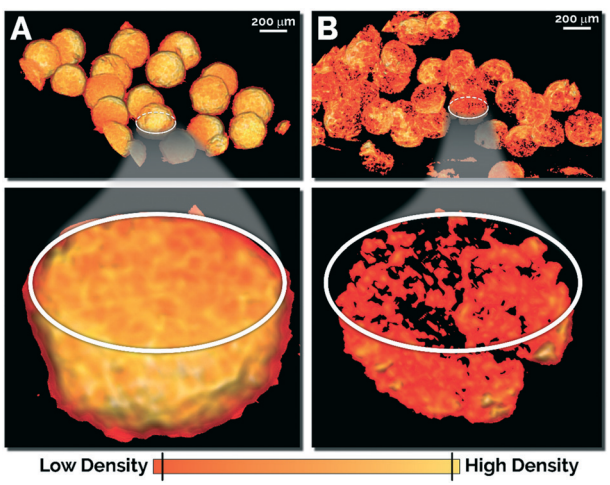

Fig. 6 Volume rendering of μCT stacked images for (A) porogen-loaded and (B) macroporous microbeads. Insets show single microbead cross-sections with identical colormaps. The microbeads were produced using Q_1 = 10 μL min^{-1}, Q_2 = 10 μL min^{-1}, and Q_3 = 300 μL min^{-1} with 5 : 1 PHMS : hexadiene ratio and 5 μm silica.

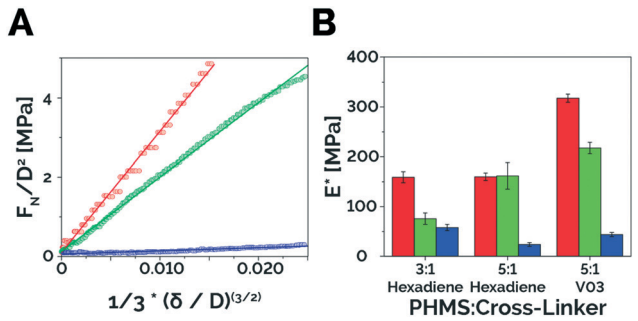

Fig. 7 (A) Low compression normalized stress *vs.* strain data for PHMS microbeads crosslinked using V03 crosslinker. (B) Effective elastic modulus for different crosslinker concentrations. A and B – Red: non-porous microbeads (control); green: silica-loaded PHMS microbeads; blue: PHMS macroporous microbeads. 3 : 1 hexadiene microbeads produced using $Q_1/Q_2/Q_3$ = 10/6/300 (5 μm silica-loaded) and 9/18/120 (control). 5 : 1 hexadiene microbeads produced using $Q_1/Q_2/Q_3$ = 10/10/300 (5 μm silica-loaded) and 5/10/200 (control). 5 : 1 V03 microbeads produced using $Q_1/Q_2/Q_3$ = 8/12/200 (5 μm silica-loaded) and 12/36/300 (control). All flowrates are in μL min^{-1}.

PHMS microbeads. As seen in Fig. 6, there is a dramatic density difference between the porogen-loaded (*i.e.*, unetched, Fig. 6A) and macroporous (*i.e.*, etched, Fig. 6B) elastomeric microbeads. The lack of high density regions within the porous microbeads suggest that the etching process is successful in selective removal of the utilized solid porogen (silica), even from the core (center) of the PHMS microbeads. As shown in Fig. 6B, the etched microbeads are primarily comprised of low-density void spaces while the silica-loaded PHMS microbeads possess high-density patches throughout the microbeads (Fig. 6B).

After confirmation of the complete selective removal of the solid porogen from the elastomeric microbeads using μCT imaging, we studied the effect of macropores on the effective modulus of the in-flow synthesized microbeads. The effective moduli of the synthesized microbeads were measured using the parallel plate test described above. A representative compression and relaxation data set is provided in the ESI† (Fig. S4). Fig. 7A shows the measured force *vs.* microbead displacement tests for porogen-free (control), porogen-loaded, and macroporous microbeads. Fig. 7B shows the calculated effective modulus of the microbeads from linear fits of force *vs.* displacement graphs (eqn (2)) similar to Fig. 7A. As seen in Fig. 7B, the porogen-free (control) microbeads had the highest effective modulus, followed by the porogen-loaded and macroporous microbeads. In addition, increasing the crosslinker concentration resulted in a more tightly bound network and thus a higher effective modulus. Furthermore, increasing the crosslinker length and elasticity (*i.e.*, V03) resulted in a stronger and more durable network, while the shorter and stiffer crosslinker (*i.e.*, hexadiene) resulted in more brittle microbeads. Particle composition (crosslinker type and ratio to the polymer) was kept constant across each group (control, silica-loaded, and etched particles) with the dripping regime maintained solely through flow rate variation.

Conclusions

In conclusion, we demonstrated the ability to continuously synthesize monodisperse elastomeric microbeads with tunable pore size and elastic modulus. The developed microfluidic platform enabled facile synthesis of porogen-loaded elastomeric microbeads with uniform loading and excellent size distribution. Increasing the size of mesoporous silica microspheres resulted in larger interconnected macropores within the elastomeric microbeads. In addition, increasing the length of the crosslinker caused a significant increase in the degree of porosity. We expect that the method presented herein will be readily extended to other linear siloxanes and functional crosslinkers with applications in areas such as adsorbents[3,24] and enzyme immobilization,[4] catalysis,[2] and tissue engineering.[6,7] The developed microbead synthesis strategy could also be applied towards the synthesis of macroporous microbeads using other substrates that can only be crosslinked chemically rather than the conventional thermal or optical triggering techniques.

Conflicts of interest

The authors declare no conflicts of interest.

Acknowledgements

The authors gratefully acknowledge the financial support provided by the National Science Foundation (Award # 1803428), and Eastman Chemical Company. We thank Prof. Saad Khan of NCSU for the use of the Rheometer in his laboratory. The authors also acknowledge the North Carolina State University Analytical Instrumentation Facility (AIF) for their assistance and the use of the Field Emission and Variable Pressure SEM and the Duke University Shared Materials Instrumentation Facility (SMIF) for use of the MicroCT.

References

1 B. Wang, P. Prinsen, H. Wang, Z. Bai, H. Wang, R. Luque and J. Xuan, *Chem. Soc. Rev.*, 2017, **46**, 855–914.
2 R. Haag and S. Roller, *Polymeric Supports for the Immobilization of Catalysts*, 2004.
3 S. Choi, T. Kwon, H. Im, D. Moon, D. J. Baek, M. Seol, J. P. Duarte and Y. Choi, *ACS Appl. Mater. Interfaces*, 2011, **3**, 4552–4556.
4 N. Miletic, Z. Vukovic, A. Nastasovic and K. Loos, *J. Mol. Catal. B: Enzym.*, 2009, **56**, 196–201.
5 R. Langer, *Nature*, 1998, **392**, 5–10.
6 A. Kumachev, J. Greener, E. Tumarkin, E. Eiser, P. W. Zandstra and E. Kumacheva, *Biomaterials*, 2011, **32**, 1477–1483.
7 S. J. Hollister, *Nat. Mater.*, 2005, **4**, 518–524.
8 S. Chatterjee, A. Potdar, S. Kuhn and G. Kumaraswamy, *RSC Adv.*, 2018, **8**, 24731–24739.
9 C. Ye, A. Chen, P. Colombo and C. Martinez, *J. R. Soc., Interface*, 2010, **7**, S461–S473.

10 A. J. Jose, S. Ogawa and M. Bradley, *Polymer*, 2005, **46**, 2880–2888.
11 D. Baah and T. Floyd-Smith, *Microfluid. Nanofluid.*, 2014, **17**, 431–455.
12 A. Khademhosseini and R. Langer, *Biomaterials*, 2007, **28**, 5087–5092.
13 P. Pospiech, J. Chojnowski, U. Mizerska, W. Fortuniak, S. Slomkowski and J. Stolarski, *Colloid Polym. Sci.*, 2017, **295**, 939–944.
14 A. Kovalenko, K. Zimny, B. Mascaro, T. Brunet and O. Mondain-monval, *Soft Matter*, 2016, **12**, 5154–5163.
15 D. Dendukuri, D. C. Pregibon, J. Collins, A. T. Hatton and P. S. Doyle, *Nat. Mater.*, 2006, **5**, 365–369.
16 S. Marre and K. F. Jensen, *Chem. Soc. Rev.*, 2010, **39**, 1183–1202.
17 Z. Wang, A. A. Volinsky and N. D. Gallant, *J. Appl. Polym. Sci.*, 2014, **41050**, 1–4.
18 A. Lamberti, S. L. Marasso and M. Cocuzza, *RSC Adv.*, 2014, **4**, 61415–61419.
19 H. Song, D. L. Chen and R. F. Ismagilov, *Angew. Chem., Int. Ed.*, 2006, **45**, 7336–7356.
20 I. Lignos, R. Maceiczyk and A. J. de Mello, *Acc. Chem. Res.*, 2017, **1**, 1248–1257.
21 V. S. Cabeza, S. Kuhn, A. A. Kulkarni and K. F. Jensen, *Langmuir*, 2012, **28**, 7007–7013.
22 S. Duraiswamy and S. A. Khan, *Nano Lett.*, 2010, **10**, 3757–3763.
23 S. Xu, Z. Nie, M. Seo, P. Lewis, E. Kumacheva, H. A. Stone, P. Garstecki, D. B. Weibel, I. Gitlin and G. M. Whitesides, *Angew. Chem.*, 2005, **117**, 734–738.
24 K. Jiang, P. C. Thomas, S. P. Forry, L. Devoe and S. R. Raghavan, *Soft Matter*, 2012, **8**, 923–926.
25 D. Chen, E. Amstad, C.-X. Zhao, L. Cai, J. Fan, Q. Chen, M. Hai, S. Koehler, H. Zhang, F. Liang, Z. Yang and D. A. Weitz, *ACS Nano*, 2017, **11**, 11978–11985.
26 E. Y. Liu, S. Jung, D. A. Weitz, H. Yi and C. Choi, *Lab Chip*, 2018, **18**, 323–334.
27 J. A. Bennett, A. J. Kristof, V. Vasudevan, J. Genzer, J. Srogl and M. Abolhasani, *AIChE J.*, 2018, **64**, 3188–3197.
28 O. Stopinski, *Platinum Group Metals*, 1977.
29 A. C. Fischer-Cripps, *Introduction to Contact Mechanics*, 2007.

